OPEN ACCESS
International Journal of Neural Systems, Vol. 31, No. 6 (2021) 2150011 (17 pages)

DOI: 10.1142/S0129065721500118

World Scientific
www.worldscientific.com

Role of the Ipsilateral Primary Motor Cortex in the Visuo-Motor Network During Fine Contractions and Accurate Performance

Camillo Porcaro*
Institute of Cognitive Sciences and Technologies (ISTC) - National Research Council (CNR), Rome, Italy
Centre for Human Brain Health and School of Psychology University of Birmingham, Birmingham, UK
S. Anna Institute and Research in Advanced Neurorehabilitation (RAN) Crotone, Italy
Department of Information Engineering - Università Politecnica delle Marche Ancona, Italy
Research Center for Motor Control and Neuroplasticity, KU Leuven Leuven, Belgium
camillo.porcaro@istc.cnr.it

Stephen D. Mayhew
Centre for Human Brain Health and School of Psychology University of Birmingham, Birmingham, UK

Andrew P. Bagshaw
Centre for Human Brain Health and School of Psychology University of Birmingham, Birmingham, UK

Accepted 10 December 2020
Published Online 18 February 2021

It is widely recognized that continuous sensory feedback plays a crucial role in accurate motor control in everyday life. Feedback information is used to adapt force output and to correct errors. While primary motor cortex contralateral to the movement (cM1) plays a dominant role in this control, converging evidence supports the idea that ipsilateral primary motor cortex (iM1) also directly contributes to hand and finger movements. Similarly, when visual feedback is available, primary visual cortex (V1) and its interactions with the motor network also become important for accurate motor performance. To elucidate this issue, we performed and integrated behavioral and electroencephalography (EEG) measurements during isometric compression of a compliant rubber bulb, at 10% and 30% of maximum voluntary contraction, both with and without visual feedback. We used a semi-blind approach (functional source separation (FSS)) to identify separate functional sources of *mu*-frequency (8–13 Hz) EEG responses in cM1, iM1 and V1. Here for the first time, we have used orthogonal FSS to extract multiple sources, by using the same functional constraint, providing the ability to extract different sources that oscillate in the same frequency range but that have different topographic distributions. We analyzed the single-trial timecourses of mu power event-related desynchronization (ERD) in these sources and linked them with force measurements to understand which aspects are most important for good task performance. Whilst the amplitude of *mu* power was not related to contraction force in any of the sources, it was able to provide

*Corresponding author.

information on performance quality. We observed stronger ERDs in both contralateral and ipsilateral motor sources during trials where contraction force was most consistently maintained. This effect was most prominent in the ipsilateral source, suggesting the importance of iM1 to accurate performance. This ERD effect was sustained throughout the duration of visual feedback trials, but only present at the start of no feedback trials, consistent with more variable performance in the absence of feedback. Overall, we found that the behavior of the ERD in iM1 was the most informative aspect concerning the accuracy of the contraction performance, and the ability to maintain a steady level of contraction. This new approach of using FSS to extract multiple orthogonal sources provides the ability to investigate both contralateral and ipsilateral nodes of the motor network without the need for additional information (e.g. electromyography). The enhanced signal-to-noise ratio provided by FSS opens the possibility of extracting complex EEG features on an individual trial basis, which is crucial for a more nuanced understanding of fine motor performance, as well as for applications in brain-computer interfacing.

Keywords: Functional source separation (FSS); semi-blind source separation (sBSS); electroencephalography (EEG); sensory-motor; contralateral primary motor (cM1); ipsilateral Primary Motor (iM1); visual feedback.

1. Introduction

A key component of human interaction with our surrounding environment is the planning and execution of motor actions to coordinate movements of the body. Grasping and manipulation of objects in a controlled and precise manner is an essential action that depends upon smooth coordination and integration of diverse sensory components such as visual cues, tactile and cutaneous feedback, grip force control and internal representations.

Neuroimaging, most commonly with functional magnetic resonance imaging (fMRI) but also magneto and electroencephalography (M/EEG), has been widely applied to study the spatio-temporal dynamics of these brain processes in an attempt to elucidate the neural origins of the sensory and cognitive components contributing to motor control.[1–5] Moreover, the organization of human motor control and knowledge of its features are fundamental for Brain–Computer Interface (BCI) implementation.[6–11]

However, two aspects have been largely neglected by previous studies which impair a full understanding. First, the majority of previous studies assume the brain activation is consistent across repeated task executions, neglecting that motor control tasks demonstrate intrinsic, between-trial variability in task performance. Understanding the neural network contributions to this variability provides a window by which the important factors influencing motor behavior can be determined, as demonstrated in our previous fMRI work.[3]

Second, with a few exceptions, the majority of previous studies have focused on understanding unimanual motor behavior by studying only task-activations in cortical, sub-cortical and cerebellar structures. The traditional view has long held that motor execution is lateralized, with the activation of the contralateral primary motor cortex (cM1) playing a dominant role. However, during unimanual motor and somatosensory tasks the activity of ipsilateral M1 (iM1) is neither quiescent nor idling but substantially perturbed by the task, typically in the form of a reduction in *mu* frequency (8–13 Hz) M/EEG power or fMRI signal below baseline levels.[12–15]

Converging evidence supports the view that the ipsilateral primary motor cortex (iM1) also contributes directly to hand and finger movements. Indeed, electrophysiological experiments have shown that, in monkeys, the activity of iM1 neurons exhibits a task-related modulation during upper limb movements.[16–20] In humans, both transcranial magnetic stimulation (TMS).[21–23] and functional imaging studies[3,12,24–26] have also concluded that iM1 contributes significantly to hand and finger movements, particularly when high dexterity is required.[12,26–30] ERD in ipsilateral motor cortex is often observed,[31,32] while TMS studies.[33–35] have indicated that during the performance of a motor task requiring fine control, the excitability of ipsilateral motor cortex is facilitated. This is not observed in tasks that do not require fine control, and is linked with reductions in inter-hemispheric inhibition from the task-active, contralateral motor cortex to the

ipsilateral motor cortex. In addition, studies combining TMS with EEG have suggested that the motor-induced *mu* ERD is an electrophysiological marker of these changes in corticospinal excitability and/or intracortical inhibition.[31,36,37]

Therefore, evidence is accumulating that iM1 can play an important role in task execution, although its precise involvement remains poorly understood. The purpose of the present EEG study is to investigate, in right-handed, healthy, young individuals, the role of iM1 during a right-hand isometric contraction against the resistance of a semi-compliant, rubber bulb either with or without visual feedback, at two levels of contraction force (30% and 10% of the maximal voluntary contraction(MVC)).

We exploit the rich information of single-trial brain responses by quantification of the quality of behavioral performance derived from recorded contraction force time series. Furthermore, we applied a semi-Blind Source Separation (s-BSS).[38–40] algorithm named Functional Source Separation (FSS) to extract distinct neural activity during visuo-motor task. The aim of FSS is to enhance the separation of relevant signals by exploiting some *a priori* knowledge without renouncing the advantages of using only information contained in original signal waveforms. Differing from other constrained ICA models,[41–43] FSS identifies a single functional source (FS) based on the contrast function that exploits *fingerprint* information associated to the neuronal pool to be identified. FSS has already demonstrated superior performance compared to other methods when extracting electrophysiological features for primary motor,[40,44] primary sensory,[40,45] primary visual[39,46] and more complex and larger network of brain regions involved in producing the P3a and P3b responses.[47,48]

Here for the first time, we have used FSS to extract multiple sources exploring orthogonal space, by using the same functional constraint, to extract three key nodes of the visuo-motor network recruited by the task, cM1, iM1 and primary visual (V1) cortex. This is a very interesting property for the orthogonal FSS, since it provides the ability to extract different sources that oscillate in the same frequency range but that have different topographic distributions.

We then identify how the differential activity between force levels, and between visually-informed motor contractions and contractions performed without visual feedback, within these three sources (cM1, iM1 and V1) contributes to the quality of behavior performance.

Overall, by exploiting information contained in behavior performance variability, with and without visual feedback, we shed further light on the integration of visual information into motor control of precision grip tasks and we elucidate the role of the iM1 in the visuomotor network.

2. Materials and Methods

2.1. *Subjects*

Seventeen right-handed subjects (age = 26 ± 4 years, 7 females) performed an isometric contraction of a pneumatic rubber bulb[49] opposing the thumb to the first two fingers of their right-hand. Handedness of every subject was assessed using the Edinburgh handedness inventory, group mean $\pm$ standard deviation = 91.8 ± 14.1. Written informed consent was obtained from all participants and the protocol was approved by the Research Ethics Board of the University of Birmingham.

2.2. *EEG recordings*

EEG signals were recorded using a 64-channel system (BrainAmp MR Plus, Brain Products, Munich, Germany). The EEG cap consisted of 62 scalp electrodes distributed according to the 10–20 system and two additional electrodes, one of which was attached approximately 2 cm below the left collarbone for recording the ECG, while the other was attached below the left eye (on the lower orbital portion of the orbicularis oculi muscle) for detection of eyeblink artefacts. Data were sampled at 5 KHz and down sampled at 1000 Hz for further analysis with FCz reference (giving a correspondence of 1 timepoint to 1 ms). Impedance at all recording electrodes was less than 10 kΩ. Off-line bandpass forward–backward filtering between 1 and 30 Hz (Butterworth second-order filter) was applied.

2.3. *Experimental procedures*

Individual's MVC of this grip was measured prior to the experiment using a mechanical hand dynamometer (0–100 kgs, Lafayette 78010, Indiana). Three trials were performed in which subject's held maximum contraction for 5 s. Their MVC was calculated

as the mean force value across trials. The pneumatic device enabled the accurate measurement of contraction force, thus enabling task performance to be quantified. An increase in the contraction force applied to the rubber bulb increased the pneumatic pressure inside a rubber tube, which was translated into an analogue electrical signal by in-house electronics and recorded by a Ni-DAQ (National Instruments).[49] Prior to the experiments, the pneumatic equipment was calibrated so that the conversion of applied force to current was known. The contraction force was continuously recorded throughout all experiments at 100 Hz sampling rate. During the experiment, subjects were instructed to maintain the isometric contraction for the 5 s trial duration at one of two force levels: either 10% or 30% of MVC. Throughout the experiment subjects were comfortably seated and viewed a visual display on a standard computer screen at a distance of 60 cm. Subjects kept their eyes open at all times and maintained fixation upon a vertical, white force-gauge that was centrally displayed upon a gray background throughout. The position of two segments aside the gauge indicated the required force (either 10% or 30% of MVC), and their appearance communicated the onset of each trial (Fig. 1).

Subjects were instructed to smoothly increase the contraction force and to then maintain this target force level as accurately as possible until the end of the trial, signaled by the disappearance of the two

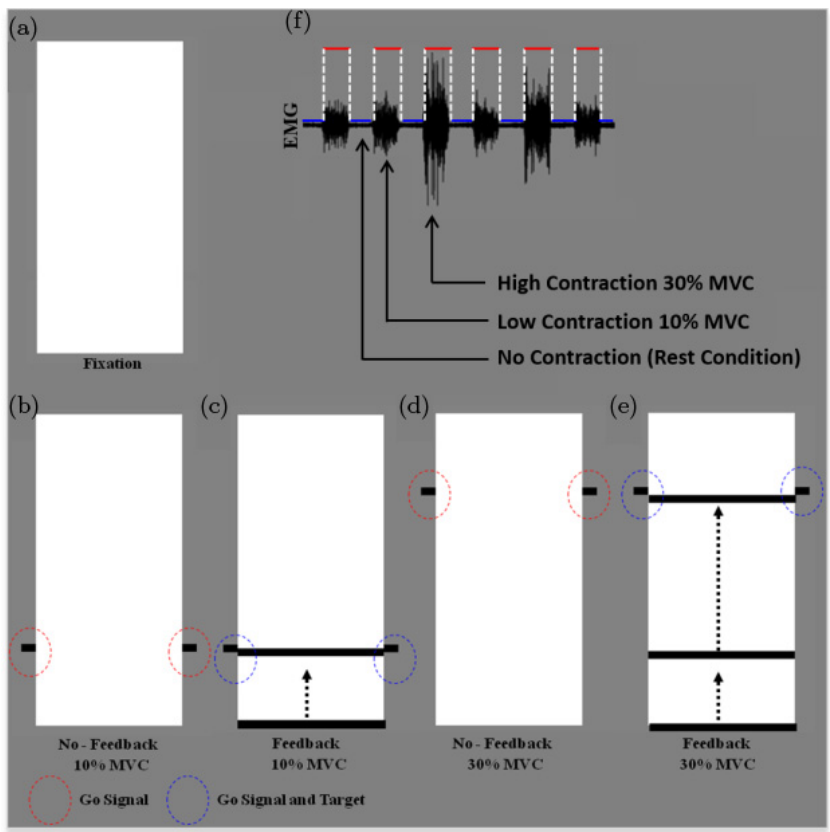

Fig. 1. Experimental design — Illustration of the visual display during the four task conditions. A rectangular white force gauge was displayed throughout all runs of the experiment and served as the resting fixation condition (A) during the 5s inter-stimulus interval. The visual displays during the whole 5 s duration of the M (10% (B) and 30% (D)) and VM (10% (C) and 30% (E)) are also shown. The trial onset GO signal was provided by the appearance of the two black side-bars instructing the target force level required in each trial. In the VM task only, a horizontal black bar indicating the current contraction force was also displayed from trial onset. This force indicator bar moved vertically up/down the screen when the subject exerted greater/lesser force to provide real-time visual feedback of task performance. The movement of the indicator bar is illustrated in the figure using dashed line arrows that were not displayed during the experiment. Electromyogram (EMG) for low, high and no contraction is also shown (F) but not displayed to the subject.

segments aside the gauge. At the trial offset, subjects were instructed to terminate the contraction and completely relax their hand and maintain central fixation on the gauge for the duration of the inter-stimulus interval lasting 5 s.

Two experimental conditions were performed as follows:

(i) Visuo-Motor (VM) condition, where a horizontal, black force indicator bar appeared centrally in the force gauge upon trial onset. The vertical position of this horizontal indicator provided continuous visual feedback information to the subject about the exerted contraction force (Fig. 1, feedback condition). The force indicator was removed from the visual display at trial offset.
(ii) Motor (M) condition, where subjects were asked to perform the isometric contraction without the display of the horizontal force indicator (Fig. 1, No Feedback condition).

During each of the VM and M tasks, 50 trials were presented for each subject, 25 for high (30% MVC) and 25 for low (10% MVC) contraction, in a pseudorandom order. Therefore, during the VM task, we acquired 25 trials of VM 10% MVC and 25 trials of VM 30% MVC. Similarly, we acquired 25 trials of M 10% MVC and 25 trials of M 30% MVC for a total of 100 trials. Isometric contractions at both force levels were executed for VM and M in two separate runs. Subjects had practised the task for a few minutes before recordings began.

3. Data Analysis

In this section, we first describe how performance was quantified on a single trial basis, before discussing the EEG analysis and the use of FSS to extract functional sources (FS) in the motor network.

3.1. *Quantification of single-trial behavioral performance*

Separately for M- and VM-tasks, single-trial force timecourses were normalized to each individual subjects' MVC to enable comparison between individuals. Single-trial force timecourses were then used to quantify subject's behavioral performance in the two tasks. In this study, we conceptualize better performance as trials where contraction force is maintained closer to the target level for the maximum time, with the minimum variation (error). Accordingly, we defined two metrics to quantify single-trial performance. We did not analyze the first 1000 ms of each trial as the data in this initial period encompassed the subject's reaction time and the time to reach the indicated level of contraction and was not informative about the stability of the contraction. We also excluded the final 500 ms so that the effects of trial offsets were not included. For each single trial T, and time point t (1 time point corresponding to 1 ms, see also Sec. 2.2 EEG Recordings), we calculated the absolute value of the error in the contraction force f as

$$\Delta F(T,t) = |f(T,t) - Q(T)|. \tag{1}$$

For the VM task, $Q(T)$ was defined as the target force, either 10% or 30% of subject's MVC. For the M-task, $Q(T)$ was defined in each trial as force attained in that trial. Therefore for the M-task, $Q(T)$ was defined, post contraction onset, as

$$Q(T) = \sum_{t \epsilon R} f(T,t)/2. \tag{2}$$

With R defined as a time range $R = \{1.0 \cdots 4.5\}$. Q is calculated for every trial summing over time in each trial.

As introduced in seminal studies investigating the role of noise in motor system control,[50] we used the coefficient of variation of the exerted pressure as a performance index. This metric has been widely used as a standardized measure of dispersion around the mean performance. This is particularly important in motor control, physiological observations show that the neural control signals are corrupted by noise whose variance increases with the size of the control signal.[51,52] In particular, isometric contractions of the hand muscles exhibit variability in force production that is proportional to the mean force exerted,[53] with the variability in continuous isometric force production thought to arise from the statistical variability and synchrony in the discharge of motor neurons supplying the muscle.[54]

The mean ($\mu\Delta F$) and standard deviation ($\sigma\Delta F$) of ΔF were calculated and the final performance metric (P_m) was defined for each trial such that the variability of the error in the contraction was normalized by the mean contraction force error:

$$P_m = \frac{\sigma\Delta F}{\mu\Delta F}. \tag{3}$$

Consequently, lower values of P_m represented better trial performance, in the form of a trial where the target force was matched more closely and with lower variability for a longer temporal period.

To visualize the relationship between P_m and behavior and to check the effectiveness of the single-trial parameterization in differentiating trials with best performance from trials with worst performance, trials were sorted by P_m values. The single trial force timecourses of each subject were sorted into lower ($Q1$ – lower values of P_m than high performance) and upper ($Q4$ – higher values of P_m than low performance) 25% quartiles separately for 10% and 30% MVC trials and both VM and M tasks. These quartiles were then used to order the corresponding EEG trials with the purpose to investigate correlations between behavior and cortical electrical activity.

Euclidean distance was also used to quantify the single trial performance to check that our results were not sensitive to the exact measure used to quantify performance. Starting from ΔF we have measure the Euclidean distance for each point of the range $R = \{1.0 \cdots 4.5\}$ as well. Lower Euclidean distance represent a closer force level to the target, 10% or 30% of the MVC for the VM task and the mean value of each trial in the range R for the M task.

3.2. *EEG data pre-processing*

EEG data were band-pass filtered (1–30 Hz) prior to further analysis using MATLAB (www.mathworks.com). A semi-automatic fastICA-based procedure[55,56] was applied to each subject to identify biological (cardiac, ocular and muscular) and nonbiological (power line, instrumental and environmental noise) artifacts, which allowed the artifacts to be removed from the signal without rejecting the contaminated epoch.

3.3. *Functional source separation*

FSS[57,58] is a semi-blind source separation method[38,39] which uses some well-known distinctive features of electrophysiological signals to inform the data decomposition. The aim of FSS is to enhance the separation of relevant signals by exploiting *a priori* knowledge without renouncing the advantages of using only information contained in the original signal waveforms. FSS, analogous to ICA, models the set of EEG signals $\mathbf{x}$ as a linear combination of an equal number of sources $\mathbf{s}$ via a mixing matrix $\mathbf{A}$ (i.e. $\mathbf{x} = \mathbf{A} \cdot \mathbf{s}$).

3.3.1. *Functional constraint*

Our study aimed to investigate the activity of the primary sensorimotor cortex FS during an isometric contraction. The functional constraint exploited *mu* (8–13 Hz) rhythmic reactivity.[14] that occurs in contralateral sensorimotor areas during unimanual motor tasks, by requiring maximal difference in *mu* spectral power between the motor conditions and rest.[59] The ad-hoc functional constraint R was defined as follows:

$$R(\mathrm{FS}) = \frac{\sum_{mu} \mathrm{PSD(Task)} - \sum_{\mathrm{mu}} \mathrm{PSD(Rest)}}{\sum_{\mathrm{mu}} \mathrm{PSD(Rest)}} \tag{4}$$

with the Power Spectrum Density (PSD) during task estimated in the 5 s contraction (both 10% MVC and 30% MVC) windows of each movement trial and at rest in the respective 5 s windows preceding each trial (*mu* ranged between 8 and 13 Hz).

3.3.2. *Orthogonal FSS extraction scheme*

To extract different sources with the same constraint we applied orthogonal FSS.[58,60] The orthogonal FSS extraction scheme was implemented in an analogous manner to the deflation version of the fastICA algorithm,[61] i.e. we extract the sources one at a time, each time we remove the extracted source before extracting the next one.

3.4. *Functional source identification*

Once the FSs were extracted (separately for the VM and M tasks), topographic distributions were obtained for both M and VM tasks. In particular, three FSs were extracted, located over motor area contralateral (cM1) and ipsilateral (iM1) to the hand isometric contraction and also a visual source (V1). To localize the sources in the brain and confirm that they represented cM1, iM1 and V1, we used an equivalent current dipole (ECD) with four concentric conductive spheres model (see routine DIPFIT2 of EEGLAB v11.0, available at http://www.sccn.ucsd.edu/eeglab). Separately for VM and M tasks, group topographic data were used

to obtain ECD positions in Montreal Neurological Institute (MNI) space, and projected them onto the MNI template.

3.5. *Functional source behavior during Visuo-Motor (VM) and Motor (M) tasks*

Once FSs (cM1, iM1 and V1) were extracted by FSS, PSD analysis was performed using the Welch approach with Hanning windows of 1024 data points. This was done separately for M and VM tasks to quantify brain activity during Rest and task (10% MVC and 30% MVC). In addition, Event Related Desynchronization (ERD.[14,62,63]) was calculated using a pre-stimulus baseline of 1 second (i.e. one second before the appearance of the *go* signal for the contraction) and 5 s post-stimulus (i.e. the duration in which the subject squeezed the rubber bulb). In particular, for both VM and M tasks we compared the ERD in the following conditions:

- 10% MVC versus 30% MVC: to investigate possible electrical brain differences in performing the two levels of isometric force contraction;
- 10% MVC versus 30% MVC for the upper (Q4) and the lower (Q1) quartiles of performance trials: to investigate possible electrical brain differences in performing the two levels of isometric force contraction depending on the performance of the task;
- Low versus high performance during 10% and 30% contractions: to investigate differences in ERD depending on the performance of the task;
- VM versus M task during lower (Q1) and upper (Q4) performance: to test behavior of the FS between the two different tasks (M and VM);

4. Statistical Analysis

For the comparisons above, we used two-sample permutation t-tests (10,000 permutations) on every frequency/point in the PSD/ERD. Kolmogorov-Smirnov test for normality indicated that PSD and ERS values among the three FSs (cM1, iM1 and V1) did not differ from a Gaussian distribution (consistently, $p > 0.200$). We used false discovery rate (FDR) to correct for multiple comparisons by using the linear-step up (LSU) procedure[64] (even though the permutation test is intrinsically robust with respect to multiple comparisons).

5. Results

All subjects successfully performed both VM and M isometric contraction tasks. The group average behavioral performance data (force level) for the VM and M tasks are plotted in Fig. 2 (top). Responses

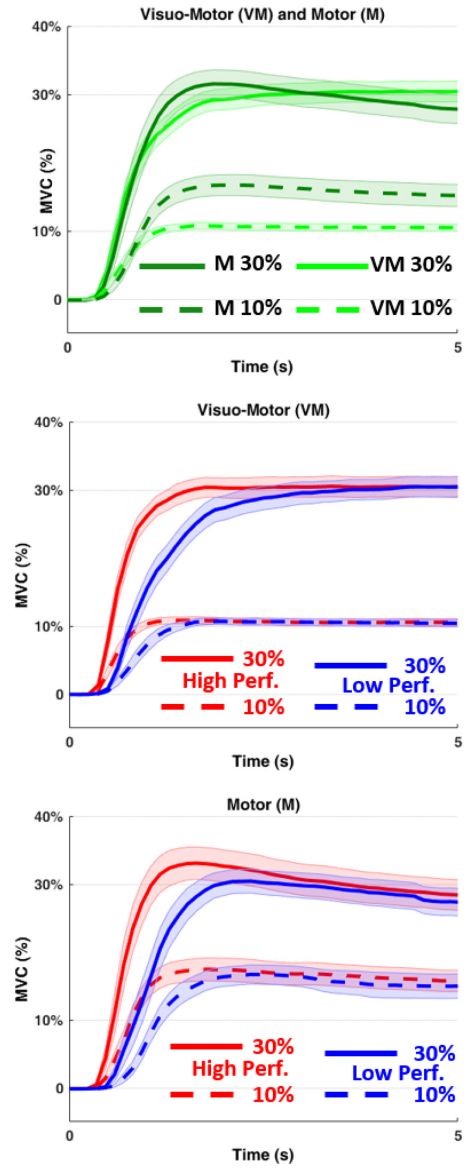

Fig. 2. Behavioral performance — Contraction force timecourses averaged across all subjects. Top — All trials averaged for the M-task (dark green) and VM-task (green) and for the 10% MVC (dashed line) and 30% MVC (continuous line). Middle — For the Visuo-Motor (VM) task higher and lower performance trials for the 30% and 10% of the MVC. Bottom — As for the Middle panel but for the Motor (M) task. The shaded area of the same colour highlights the standard error.

to both tasks featured an approximately 1000 ms delay before the contraction force increased from pre-stimulus baseline levels. Of note, during the M 10% MVC task only, the subjects tended to overestimate the required force level.

No significant difference in subjects' mean stable contraction force was observed between VM- and M-tasks for either 10% ($p = 0.82$) or 30% trials ($p = 0.62$, paired t-tests), indicating that the contraction force was comparable with and without feedback. MVC was consistent across subjects, group mean ± standard deviation = 9.7±1.4 kg; range = 7.25–12 kg. No linear correlation was observed between subjects' MVC and mean performance measure (P_m across trials for any condition: 10% VM ($R = 0.31$, $p = 0.21$); 30% VM ($R = 0.08$, $p = 0.70$); 10% M ($R = 0.19$, $p = 0.47$); 30% M ($R = 0.21$, $p = 0.42$).

Furthermore, no correlation was observed between MVC and mean maximum contraction force for either 10% ($R = -0.04$, $p = 0.88$) or 30% trials ($R = -0.25$, $p = 0.32$) indicating that subject's MVC did not determine their performance.

The group average of trials sorted into lower and upper quartiles of P_m for 10% and 30% contractions are displayed in Fig. 2 (middle and bottom, respectively, for Visuo-Motor and Motor Task). In particular, good performance could be qualitatively identified by: faster response time, matching of the contraction force to the target force with less error and therefore greater accuracy and stability, and longer duration maintenance of steady contraction. In the VM-task, lower and upper quartiles of P_m displayed equivalent contraction force levels during the stable period (approximately 2–5 s), indicating that subjects consistently attained the target force. No differences in the mean force level during the stable period of contraction were observed between upper and lower quartiles of P_m in the M-task. The error in the contraction maintenance during the upper quartiles was considerably larger than observed in the VM-task.

5.1. *Properties of identified functional sources*

FSS successfully extracted three main sources: Contralateral Motor (cM1), Ipsilateral Motor (iM1) and Visual (V1) in both conditions (VM and M). Figure 3 shows group topography and PSD, compared between rest and task, for each source and each

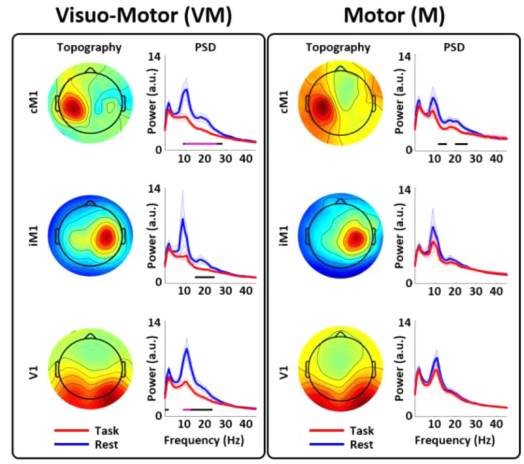

Fig. 3. Functional Sources Behavior — Grand average topography and power spectrum density (PSD) for the three FSs (cM1, iM1 and V1) are shown for VM and M tasks. The shaded area around the solid line highlights the standard error. The horizontal black line indicates a significant group difference between task (red) and rest (blue) conditions (permutation t-test at $p < 0.05$; horizontal pink line indicates pFDR < 0.05).

condition. A clear decrease in *mu* power (decrease in power from rest to task) in the contralateral source was seen during both the VM task ($p < 0.05$, FDR corrected) and M task ($p < 0.05$). A desynchronization was observed in iM1 during the VM task, although only in the beta band did this reach significance ($p < 0.05$, as shown by the horizontal black line in Fig. 3, second row left). Desynchronization of *mu* activity also occurred for the visual source. In contrast, for the M condition neither ipsilateral nor visual FS showed significant desynchronization, nor was here a substantial qualitative difference between task and rest.

Figure 4 shows the localized activity within the MNI template for each source and for each condition. MNI coordinates and Brodmann Areas (BAs) are also reported in Fig. 4.

5.2. *Event related desynchronization differences in response to contractions between experimental conditions*

5.2.1. *Low contraction (10% MVC) versus high contraction (30% MVC) functional source behavior*

The level of contraction force was not a significant modifier of ERD in any of the sources (see Fig. 5).

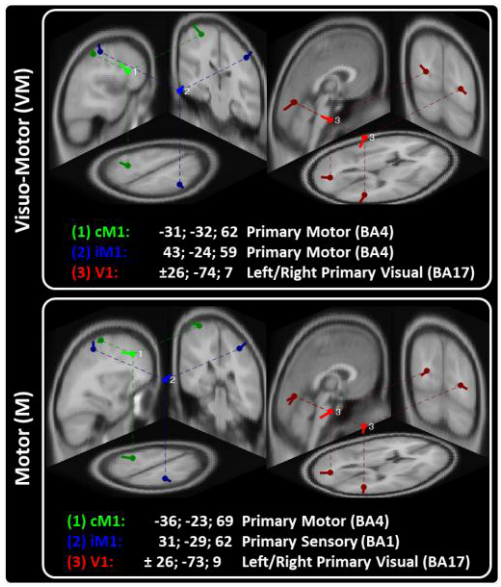

Fig. 4. Source positions — Position and orientation of the ECD for VM and M tasks for the three FSs (cM1, green; iM1, blue and V1, red), superimposed on the Montreal Neurological Institute (MNI) brain template in axial, coronal, and sagittal views. For each source MNI (x, y, z) coordinates are shown as well as BAs.

This was true even when we compared trials with the best versus the worst performance of the task (see Appendix A. Supplementary figures, Fig. S1).

5.2.2. *High performance versus low performance contraction accuracy during VM and M Tasks*

While force was not predictive of ERD in any of the sources, performance was (see Fig. 6). There were, in particular, differences in the behavior of the ipsilateral source (iM1) between the VM and M tasks. During both contraction levels (10% and 30% MVC) of the VM task, the iM1 source showed a greater magnitude ERD (i.e. lower power) during higher accuracy trials compared to lower accuracy trials. This difference was present throughout the contraction period. On the other hand, cM1 primarily showed a significant difference between higher and lower performance during the first second after the onset of the 30% MVC contraction. In the M-task, cM1 and iM1 showed similar behavior, with significantly greater ERD in high performance compared to low performance trials during the first second of the 30% contraction. No differences related to performance were observed for the visual functional source (V1) for any of the conditions or tasks.

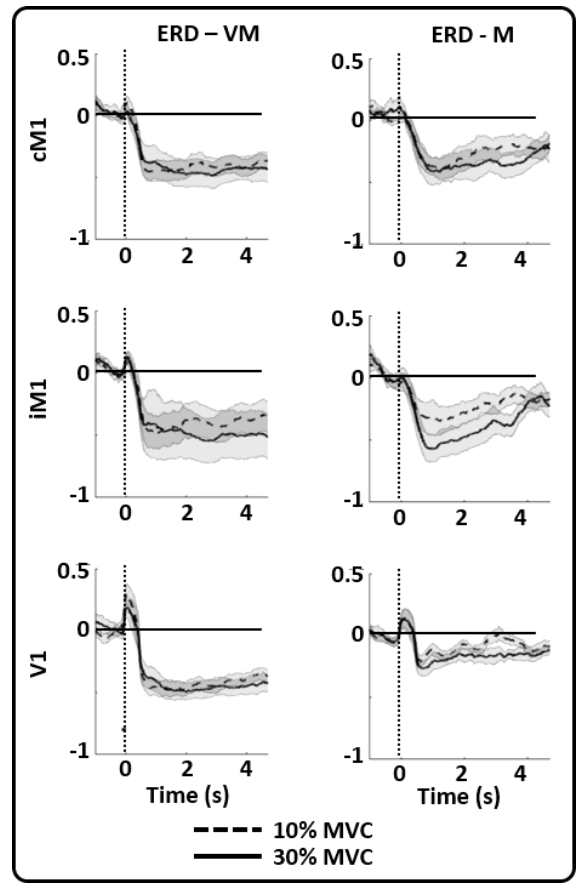

Fig. 5. Low contraction (10% MVC) versus high contraction (30% MVC) FS behavior. ERD for VM (left column) and M (right column) conditions are shown for the three FSs extracted (cM1, iM1 and V1). The shaded area highlights standard error. The dashed line refers to 10% and continuous line refers to 30% of the MVC.

5.2.3. *Visuo-Motor (VM) versus Motor (M) task functional behavior*

A direct comparison between the VM and M tasks showed interesting differences in source activity in both the 10% and 30% MVC contractions and for both performance measures used $\boldsymbol{P_m}$ and Euclidean distance (see Appendix A. Supplementary figures, Fig. S2 for the results obtained using Euclidean distance). Figure 7 shows the same data as Fig. 6, but organized to compare source ERD between, rather than within, M and VM tasks. The first row (A, B) of Fig. 7 shows differences between VM and M tasks in the three FSs (cM1, iM1 and V1). In particular, and

as might be expected, the visual FS was most different between the VM and M tasks (pFDR < 0.05, A and B). At both levels of contraction, a larger magnitude ERD of the visual source was seen in the VM task, compared to the M task.

Subdividing the trials with respect to the motor performance revealed differences in the source activity between the two tasks, particularly for the ipsilateral source (see Figs. 7(C)–7(F) and S1). In particular, for both levels of contraction (10% and 30% MVC) the ERD was maintained at a constant level throughout the whole contraction for the VM task, whereas for the M task after reaching a similar magnitude ERD it steadily returned to baseline. Of note, in lower performance accuracy trials the VM and M source behaved similarly, with a rapid return to baseline power levels during the period of contraction. This indicates that during low accuracy VM trials, the ipsilateral source exhibited behavior closely resembling that observed during the M task

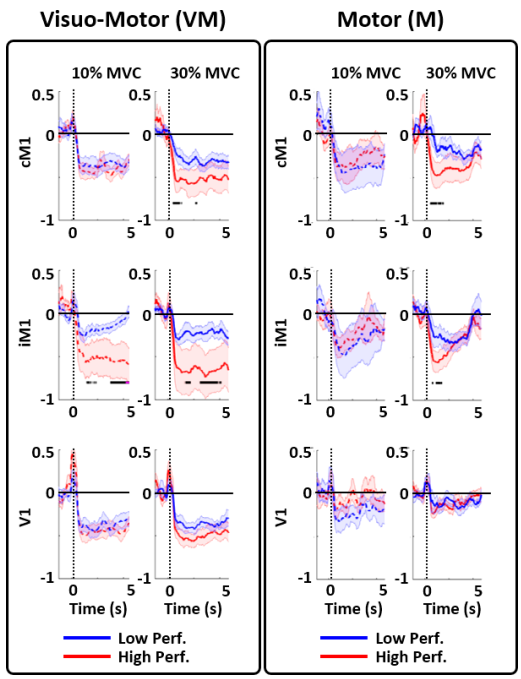

Fig. 6. Low performance versus high performance contraction accuracy. ERD for VM – (left quadrant) and M (right quadrant) conditions are shown for 10% MVC (first column) and 30% MVC (second column) for the three FSs (cM1, iM1 and V1) extracted. The shaded area of the same colour highlights the standard error. The horizontal black line indicates a significant group difference between higher (red) and lower (blue) performance (permutation t-test at $p < 0.05$).

(Figs. 7(C)–7(D), middle column). Highly comparable results were observed when using the Euclidean distance measure of performance (Fig. S2). In addition, whilst the magnitude of the ERD alone is not very informative of behavioral quality or task type, the temporal pattern of the ERD is.

For the contralateral source, the differences in ERD observed during the 10% MVC for all trials turned out to be driven by the higher accuracy trials (Figs. 7(E) and S2). No differences were observed between the contralateral source behavior during low performance trials (Figs. 7(C), 7(D) and S2).

Finally, the visual FS was strongly involved at both contraction levels (10% and 30% MVC) and able to differentiate the VM task from the M task, as discussed above. It was also affected by the accuracy of the contraction (see Figs. 7(C)–7(F) and S2). While generally having similar time-courses over the period of contraction, the difference between VM and M tasks was most clear for high accuracy trials.

The same data as for Fig. 6 but organized to compare source ERD between, rather than within, M and VM tasks. The three rows show data for all trials together, the low and high performance trials, respectively. The shaded area of the same color highlights the standard error, while the horizontal black line indicates a significant group difference between VM and M conditions (permutation t-test at $p < 0.05$; horizontal pink line indicates pFDR < 0.05).

6. Discussion

Understanding the mechanisms underlying fine motor control is crucial, not only for basic scientific knowledge but also to optimize rehabilitation strategies following brain injury or in relation to aging.[65–69] A clearer understanding of the scalp EEG signatures of motor control is also particularly crucial for the development of brain-computer interfaces, which often rely on EEG because of its temporal resolution, and ease of use.[22,70–72] In this study, we used EEG data enhanced by FSS (extracting sources maximizing task versus rest changes in *mu* activity) to characterize the electrophysiological behavior of the brain regions relevant for the fine control of isometric hand contractions performed both with and without visual feedback. Measurements of

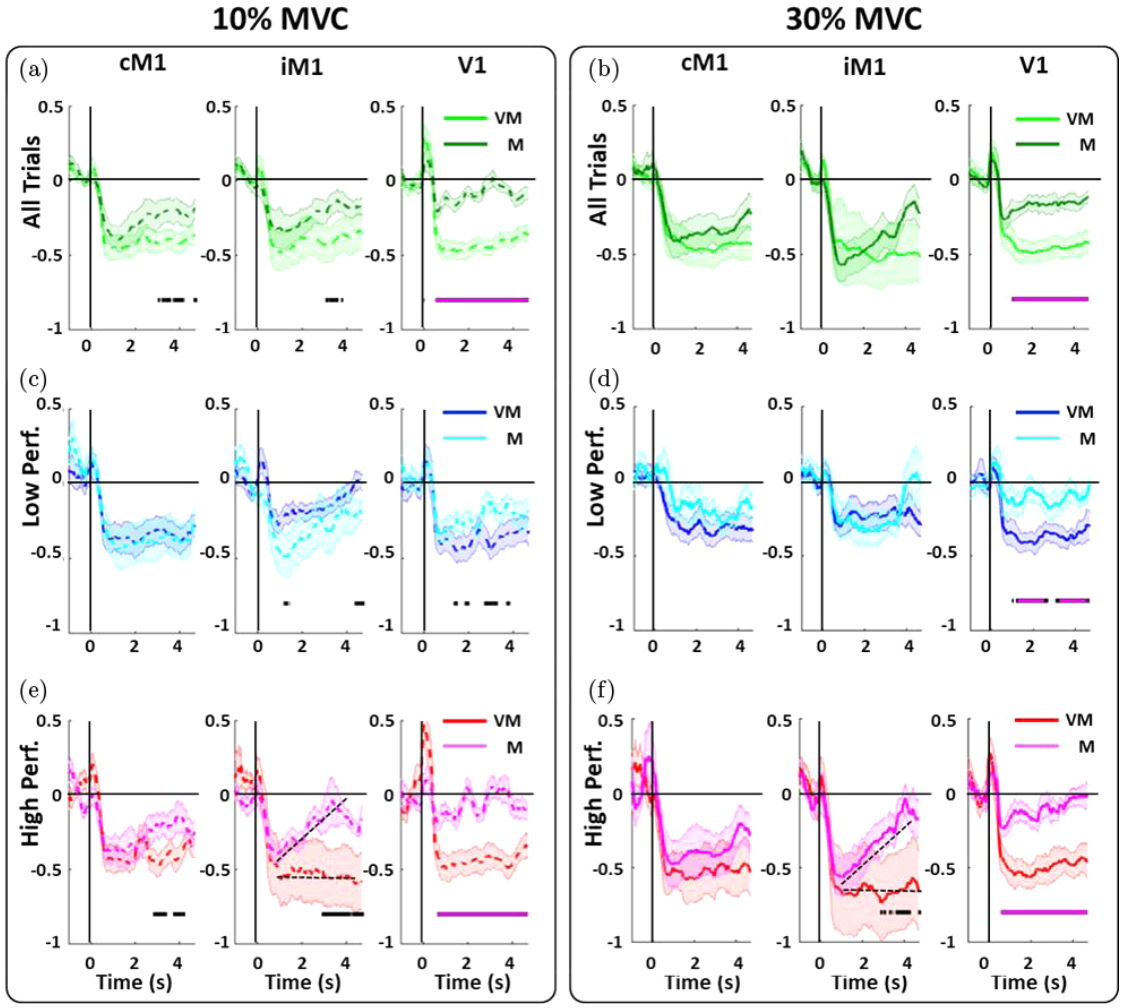

Fig. 7. VM versus M Condition and contraction performance. The same data as for Fig. 6 but organized to compare source ERD between, rather than within, M and VM tasks. The three rows show data for all trials together, the low and high performance trials respectively. The shaded area of the same colour highlights the standard error, while the horizontal black line indicates a significant group difference between VM and M conditions (permutation t-test at $p < 0.05$; horizontal pink line indicates pFDR < 0.05).

mu ERD alongside single trial metrics of behavioral performance were used to elucidate the low-frequency neural mechanisms underlying fine motor control in healthy volunteers. This analysis enabled us to identify ipsilateral primary motor cortex (iM1) as the FS most strongly associated with accurately maintaining a stable and precise isometric contraction under conditions of visual feedback. While the other nodes of the visuomotor network were necessary for performance of the task in both conditions (with and without visual feedback), only the activity of iM1 was able to differentiate between high and low performance trials when there was visual feedback. Our approach requires only EEG data to identify and characterize the motor network nodes. It is hence more straightforward and widely applicable than methods based on corticomuscular coherence,[8,9] as well as having the advantage that it can characterize the network more broadly beyond cM1.[40,61]

In addition, studies combining TMS with EEG have suggested that the motor-induced *mu* ERD is an electrophysiological marker of these changes in corticospinal excitability and/or intracortical inhibition.[31,36,37] Our results demonstrate that these changes in excitatory and inhibitory tone within the motor network are associated with trial-by-trial variability in behavioral performance. Furthermore,

using the enhanced signal-to-noise ratio and specificity facilitated by FSS, this detailed knowledge of the dynamic state of the motor network can be accessed noninvasively using scalp EEG.

The majority of our current knowledge concerning the brain regions recruited by motor tasks comes from analyses that assume brain activation is consistent across repeated task executions. Such an approach neglects the fact that motor control tasks demonstrate considerable intrinsic, between-trial variability in aspects such as response speed and the magnitude, duration, accuracy and stability of contraction force. All of these factors contribute to variations in the quality of overall task performance, but this has largely been attributed to noise that corrupts motor commands.[77] However, motor studies, as well as those in other sensory modalities, have shown clearly that trial-by-trial variability contains perceptually and behaviorally relevant information that can be crucial to provide a full understanding of the temporal dynamics of network activity.[3,74–79] This point is made clearly in our data, since even when the subject was instructed to maintain the contraction level, both sensor pressure and the magnitude of the ERD decreased through the contraction period, particularly in the low force and no feedback tasks (Figs. 5 and 6). By using this variability and sorting trials according to task performance we were able to demonstrate that the involvement of iM1 is crucial for the stable and consistent maintenance of the target force level. Of the nodes investigated, the behavior of iM1 was most impacted by differences in performance, with a strong and sustained ERD observed throughout the contraction period, for both force levels, during high performance VM trials. The temporal evolution of the ERD in low performance VM trials was much more comparable to that in M trials, with a gradual return to baseline during the contraction period. By comparison, despite their clear importance in the performance of both tasks, cM1 and V1 were much less informative about the quality of task performance. The data clearly suggested that higher behavioral performance involved a sustained and pronounced ERD in iM1, but was less dependent on cM1. However, it is worth noting that even within trials with a high level of performance, there is considerable variability in the ERD in iM1, and in many cases this variability is larger than for cM1 and V1. This can be seen by comparing the shaded areas for iM1, cM1 and V1 representing the standard error across trials, in for example Fig. 6. ERD of iM1 has previously been found to correlate relatively weakly with corticospinal tract excitability, measured using TMS,[31] and with simultaneously recorded fMRI responses.[80] It is possible that these correlations will be improved by the higher signal-to-noise ratio provided by FSS compared to other source modeling approaches or the use of electrode space data. This will need to be examined in future work. However, for truly single-trial applications of iM1 ERD (e.g. BCI) more understanding is needed of the sources of this variability, the link between iM1 ERD and task performance, and of the dynamics of the entire motor network.

We have previously taken a similar single-trial approach with the same task using fMRI data.[3] Consistent with the current studies observation of greater ipsilateral excitability during best performance, during fMRI we found that high performance trials were associated with increased blood oxygenation level dependent (BOLD) signal (smaller magnitude deactivations) in ipsi-lateral M1 compared to low performance trials. In terms of the BOLD signal associated with a unilateral motor task, ipsilateral M1 generally demonstrates a negative response, a decrease below pre-stimulus baseline levels, but our previous results suggest increased recruitment of ipsilateral M1 is beneficial for task performance. Our fMRI results also demonstrated wider recruitment of several other regions within the motor network for which an increase in BOLD signal was associated with improved performance.[3] These observations with the same task performed using EEG and fMRI therefore provide convergent evidence to support the role of ipsilateral M1 when fine motor control is needed. In light of the previously-discussed TMS studies, this presumably represents reduced inter-hemispheric inhibition from contra-lateral to ipsi-lateral M1, allowing ipsilateral M1 to be involved in task performance. This viewpoint is shared by other recent fMRI studies that advocated the involvement of iM1 in motor control[12,26] and a recent review[81] has discussed how activation of the ipsilateral hemisphere can entail processes that serve to suppress interhemispheric cross-talk through transcallosal tracts. Therefore, taken together, our results correspond with and add to the emerging consensus that bi-hemispheric activation occurs to support

completion of lateralized motor tasks, particularly when there is visual feedback.

While providing new approaches to understand the electrophysiological correlates of fine motor performance, this work has some important limitations for future studies to address. In particular, a more specific and detailed investigation of how the three sources interact is needed. While we adopted an approach based on quantifying single-trial variability, we relied upon averaging of subsets of trials, ordered according to performance accuracy. A more direct investigation of the effects we observed and the ability of the measures we extracted to be informative for individual trials (e.g. for BCI applications) will be needed.

While our focus on the *mu* rhythm was motivated by its obvious involvement in motor control, future work will also need to extend our findings to other frequencies. In particular, the beta band is often implicated in motor control, while gamma band activity as a signature of local processing will be particularly important to link with our *mu* observations. In addition, it is important to remember that EEG has limited sensitivity to subcortical structures (e.g. basal ganglia, thalamus) which are also known to play a key role in motor control.[82–84] Integration of EEG with fMRI could help to elucidate the underlying mechanisms of fine control movement and task performance with higher spatiotemporal accuracy.

7. Conclusion

This work has developed and applied the FSS approach to allow the extraction of multiple sources within an orthogonal space. Sequential application of the same functional constraint was able to extract the key nodes of the network, allowing investigation of their behavior in relation to task performance. By quantifying the motor network dynamics underlying inter-trial variability we have demonstrated the crucial role played by iM1 in controlling fine movements, and in particular the accuracy of the contraction performance and maintenance of the steady level of the contraction under conditions with visual feedback. The ability to extract these sources from EEG data alone, accurately and in a data driven manner with minimal assumptions, opens up new possibilities for understanding and quantifying the motor system in health and pathology.

Acknowledgments

We thank the following sources for funding this research. Engineering and Physical Science Research Council (EPSRC), APB: EP/F023057/1; The Royal Society International Joint Project – 2010/R1; SDM was funded by an EPSRC Fellowship (EP/I022325/1) and a Birmingham Fellowship.

Appendix A. Supplementary Figures

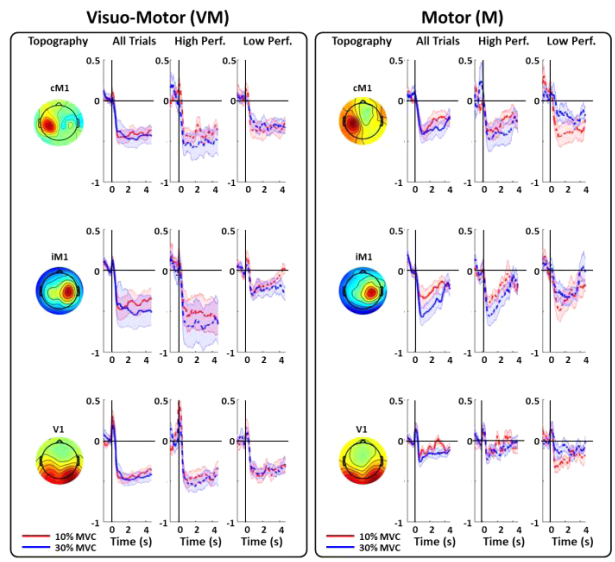

Fig. S1. Low contraction (10% MVC) versus high contraction (30% MVC) FS behavior (low versus high performance). Grand average topographic map (as shown in Fig. 3) and ERD for VM– (left column) and M (right column) conditions, for the three FSs extracted (cM1, iM1 and V1). The shaded area highlights standard error. ***All trials*** columns represents ERD as shown in Fig. 5 where red line refers to 10% and blue line refers to 30% of the MVC. ***High Perf.*** column shows ERD for the higher performance trials and ***Low perf.*** column shows ERD for the lower performance trials. No significant differences were observed between VM and M conditions for ***All trials*** (as shown in Fig. 5) or between higher and lower performance trials.

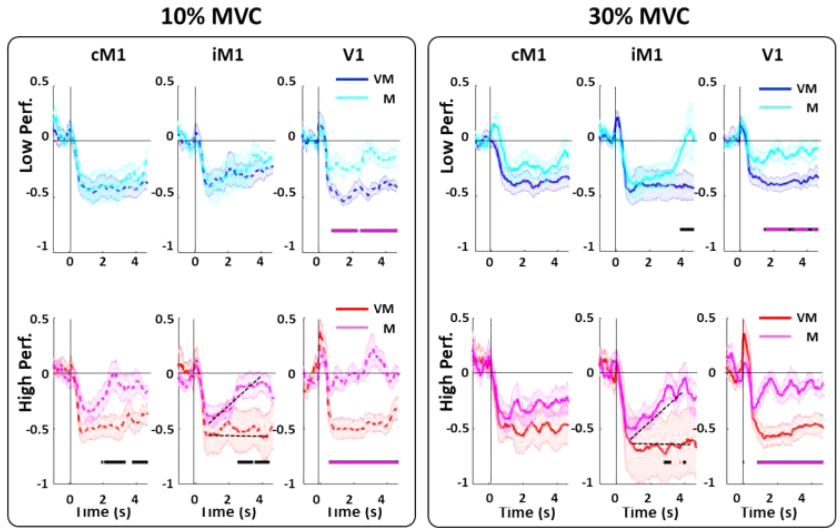

Fig. S2. VM versus M Condition and contraction performance by Euclidean distance. Here we shows the results obtained using as a performance measure the Euclidean distance. The two rows show data for low (top row) and high performance trials (bottom row). The shaded area of the same colour highlights the standard error, while the horizontal black line indicates a significant group difference between VM and M conditions (permutation t-test at $p < 0.05$; horizontal pink line indicates pFDR < 0.05).

References

1. M. Bourguignon, H. Piitulainen, E. Smeds *et al.*, MEG insight into the spectral dynamics underlying steady isometric muscle contraction, *J. Neurosci.* **37**(43) (2017) 10421–10437.
2. M. Jochumsen, C. Rovsing, H. Rovsing, I. K. Niazi, K. Dremstrup and E. N. Kamavuako, Classification of Hand Grasp Kinetics and Types Using Movement-Related Cortical Potentials and EEG Rhythms. *Comput. Intell. Neurosci.* **2017** (2017) 7470864, doi: 10.1155/2017/7470864.
3. S. D. Mayhew, C. Porcaro, F. Tecchio and A. P. Bagshaw, fMRI characterisation of widespread brain networks relevant for behavioral variability in fine hand motor control with and without visual feedback, *Neuroimage* **148** (2017) 330–342, doi: 10.1016/j.neuroimage.2017.01.017.
4. E. Pirondini, M. Coscia, J. Minguillon, J. D. R. Millán, D. Van De Ville and S. Micera, EEG topographies provide subject-specific correlates of motor control, *Sci Rep.* **17**(1) (2017) 13229, doi: 10.1038/s41598-017-13482-1.
5. L. Cheng, Y. Zhu, J. Sun, L. Deng, N. He, Y. Yang, H. Ling, H. Ayaz, Y. Fu and S. Tong, Principal states of dynamic functional connectivity reveal the link between resting-state and task-state brain: An fMRI study, *Int. J. Neural. Syst.* **28**(7) (2018) 1850002, doi: 10.1142/S0129065718500028.
6. A. Ortiz-Rosario and H. Adeli, Brain-computer interface technologies: From signal to action, *Rev. Neurosci.* **24**(5) (2013) 537–552, doi: 10.1515/revneuro-2013-0032.
7. A. Burns, H. Adeli and J. A. Buford, Brain-computer interface after nervous system injury, *Neurosci.* **20**(6) (2014) 639–651, doi: 10.1177/1073858414549015.
8. A. Chowdhury, H. Raza, Y. K. Meena *et al.*, An EEG-EMG correlation-based brain-computer interface for hand orthosis supported neuro-rehabilitation, *J. Neurosci. Methods* **312** (2019) 1–11, doi: 10.1016/j.jneumeth.2018.11.010.
9. A. Chowdhury, H. Raza, A. Dutta *et al.*, A study on cortico-muscular coupling in finger motions for exoskeleton assisted neuro-rehabilitation, in *Annu. Int Conf. IEEE Eng. Med. Biol. Soc.* (2015), doi: 10.1109/EMBC.2015.7319421.
10. A. Ortiz-Rosario, I. Berrios-Torres, H. Adeli and J. A. Buford, Combined corticospinal and reticulospinal effects on upper limb muscles, *Neurosci. Lett.* **561** (2014) 30–34.
11. A. Ortiz-Rosario, H. Adeli and J. A. Buford, Wavelet methodology to improve single unit isolation in primary motor cortex cells, *J. Neurosci. Methods* **246** (2015) 106–118.
12. T. Verstynen, J. Diedrichsen, N. Albert *et al.*, Ipsilateral motor cortex activity during unimanual hand movements relates to task complexity, *J. Neurophysiol.* **93**(3) (2005) 1209–1222.
13. T. Verstynen and R. B. Ivry, Network dynamics mediating ipsilateral motor cortex activity during unimanual actions, *J. Cogn. Neurosci.* **23**(9) (2011) 2468–2480.
14. G. Pfurtscheller and F. H. Lopes, Event-related EEG/MEG synchronization and desynchronization:

Basic principles, *Clin. Neurophysiol.* **110** (1999) 1842–1857.
15. C. Neuper, M. Wortz and G. Pfurtscheller, ERD/ERS patterns reflecting sensorimotor activation and deactivation. Event-Related Dyn, *Brain Oscil.* **159** (2006) 211–222.
16. J. Tanji, K. Okano and K. C. Sato, Neuronal activity in cortical motor areas related to ipsilateral, contralateral, and bilateral digit movements of the monkey, *J. Neurophysiol.* **60**(1) (1988) 325–343.
17. O. Donchin, A. Gribova, O. Steinberg *et al.*, Primary motor cortex is involved in bimanual coordination, *Nature* **395** (1998) 274–278.
18. O. Kazennikov, B. Hyland, M. Corboz *et al.*, Neural activity of supplementary and primary motor areas in monkeys and its relation to bimanual and unimanual movement sequences, *Neurosci.* **89** (1999) 661–674.
19. O. Steinberg, O. Donchin, A. Gribova *et al.*, Neuronal populations in primary motor cortex encode bimanual arm movements, *Eur. J. Neurosci.* **15**(8) (2002) 1371–1380.
20. P. Cisek, D. J. Crammond and J. F. Kalaska, Neural activity in primary motor and dorsal premotor cortex in reaching tasks with the contralateral versus ipsilateral arm, *J. Neurophysiol.* **89** (2003) 922–942.
21. A. Stedman, N. J. Davey and P. H. Ellaway, Facilitation of human first dorsal interosseous muscle responses to transcranial magnetic stimulation during voluntary contraction of the contralateral homonymous muscle, *Muscle Nerve* **21**(8) (1998) 1097–4598.
22. M. Tinazzi and G. Zanette, Modulation of ipsilateral motor cortex in man during unimanual finger movements of different complexities, *Neurosci. Lett.* **244**(3) (1998) 121–124.
23. M. Davare, J. Duque, Y. Vandermeeren *et al.*, Role of the ipsilateral primary motor cortex in controlling the timing of hand muscle recruitment, *Cereb. Cortex* **17**(2) (2007) 353–362.
24. S. G. Kim, J. Ashe, K. Hendrich *et al.*, Functional magnetic resonance imaging of motor cortex: Hemispheric asymmetry and handedness, *Science* **261**(5121) (1993) 615–617.
25. S. C. Cramer, S. P. Finklestein, J. D. Schaechter *et al.*, Activation of distinct motor cortex regions during ipsilateral and contralateral finger movements, *J. Neurophysiol.* **81**(1) (1999) 383–387, doi: 10.1152/jn.1999.81.1.383.
26. J. Diedrichsen, T. Wiestler and J. W. Krakauer, Two distinct ipsilateral cortical representations for individuated finger movements, *Cereb. Cortex* **23**(6) (2013) 1362–1377.
27. N. Sadato, G. Campbell, V. Ibáñez *et al.*, Complexity affects regional cerebral blood flow change during sequential finger movements, *J. Neurosci.* **16**(8) (1996) 2691–2700.
28. M. J. Catalan, M. Honda, R. A. Weeks *et al.*, The functional neuroanatomy of simple and complex sequential finger movements: A PET study, *Brain* **121** (1998) 253–264, doi: 10.1093/brain/121.2.253.
29. F. Hummel, Kirsammer and C. Gerloff, Ipsilateral cortical activation during finger sequences of increasing complexity: Representation of movement difficulty or memory load? *Clin. Neurophysiol.* **114**(4) (2003) 605–613.
30. E. Berlot, G. Prichard, J. O'Reilly *et al.*, Ipsilateral finger representations in the sensorimotor cortex are driven by active movement processes, not passive sensory input, *J. Neurophysiol.* **121**(2) (2019) 418–426.
31. K. Hasegawa, S. Kasuga, K. Takasaki *et al.*, Ipsilateral EEG mu rhythm reflects the excitability of uncrossed pathways projecting to shoulder muscles, *J. Neuroeng. Rehabil.* **14**(1) (2017) 85, doi: 10.1186/s12984-017-0294-2.
32. H. Yuan, C. Perdoni, L. Yang and B. He, Differential electrophysiological coupling for positive and negative BOLD responses during unilateral hand movements, *J. Neurosci.* **31**(26) (2011) 9585–9593.
33. G. A. Ghacibeh, R. Mirpuri, V. Drago *et al.*, Ipsilateral motor activation during unimanual and bimanual motor tasks, *Clin. Neurophysiol.* **118**(2) (2007) 325–332.
34. T. Morishita, K. Uehara and K. Funase, Changes in interhemispheric inhibition from active to resting primary motor cortex during a fine-motor manipulation task, *J. Neurophysiol.* **107**(11) (2012) 3086–3094.
35. T. Morishita, M. Ninomiya, K. Uehara and K. Funase, Increased excitability and reduced intracortical inhibition in the ipsilateral primary motor cortex during a fine-motor manipulation task, *Brain Res.* **1371** (2011) 65–73.
36. C. Rau, C. Plewnia, F. Hummel and C. Gerloff, Event-related desynchronization and excitability of the ipsilateral motor cortex during simple self-paced finger movements, *Clin. Neurophysiol.* **114**(10) (2003) 1819–1826.
37. M. Takemi, Y. Masakado, M. Liu and J. Ushiba, Event-related desynchronization reflects downregulation of intracortical inhibition in human primary motor cortex, *J. Neurophysiol.* **110**(5) (2013) 1158–1166.
38. C. Porcaro and F. Tecchio, Semi-blind functional source separation algorithm from non-invasive electrophysiology to neuroimaging, in *Blind Source Separation: Advances in Theory, Algorithms and Applications*, eds. G. R. Naik, W. Wang (Springer, Berlin, Heidelberg, 2014), pp. 521–551.
39. C. Porcaro, D. Ostwald, A. Hadjipapas *et al.*, The relationship between the visual evoked potential and the gamma band investigated by blind and semi-blind methods, *Neuroimage* **56**(3) (2011) 1059–1071.

40. C. Porcaro, C. Cottone, A. Cancelli *et al.*, Functional semi-blind source separation identifies primary motor *Area Without Active Motor Execution*, *Int. J. Neural Syst.* **28**(3) (2018) 1750047, doi: 10.1142/S0129065717500472.
41. S. Ferdowsi, S. Sanei and V. Abolghasemi, A predictive modeling approach to analyze data in EEG-fMRI experiments, *Int. J. Neural Syst.* **25**(1) (2015) 1440008.
42. O. I. Khan, F. Farooq, F. Akram *et al.*, Robust extraction of P300 using constrained ICA for BCI applications, *Med. Biol. Eng. Comput.* **50**(3) (2012) 231–241.
43. W. Lu and J. C. Rajapakse, Approach and applications of constrained ICA, *IEEE Trans. Neural Networks* **16**(1) (2005) 203–212.
44. C. Porcaro, G. Barbati, F. Zappasodi *et al.*, Hand sensory-motor cortical network assessed by functional source separation, *Hum. Brain Mapp.* **29**(1) (2008) 70–81.
45. C. Porcaro, G. Coppola, Lorenzo G Di *et al.*, Hand somatosensory subcortical and cortical sources assessed by functional source separation: An EEG study, *Hum. Brain Mapp.* **30**(2) (2009) 660–674.
46. C. Porcaro, D. Ostwald and A. P. Bagshaw, Functional source separation improves the quality of single trial visual evoked potentials recorded during concurrent EEG-fMRI, *Neuroimage* **50**(1) (2010) 112–123.
47. C. Porcaro, J. H. Balsters, D. Mantini *et al.*, P3b amplitude as a signature of cognitive decline in the older population: An EEG study enhanced by Functional Source Separation, *Neuroimage* **181** (2019) 535–546.
48. F. Ferracuti, V. Casadei, I. Marcantoni *et al.*, A functional source separation algorithm to enhance error-related potentials monitoring in noninvasive brain-computer interface, *Comput. Methods Programs Biomed.* **191** (2020) 105419.
49. B. C. M. Van Wijk, A. Daffertshofer, N. Roach and P. Praamstra, A role of beta oscillatory synchrony in biasing response competition? *Cereb. Cortex* **19**(6) (2009) 1294–1302, doi: 10.1093/cercor/bhn174.
50. M. W. Daniel and C. M. Harris, Signal Dependent Noise Determines Motor Planning, *Nature* **394** (1998) 780–784.
51. T. Brashers-Krug, R. Shadmehr and E. Bizzi, Consolidation in human motor memory, *Nature* **382**(6588) (1996) 252-255, doi: 10.1038/382252a0.
52. R. Shadmehr and F. A. Mussa-Ivaldi, Adaptive representation of dynamics during learning of a motor task, *J. Neurosci.* **14**(5) (1994) 3208–3224.
53. K. E. Jones, A. F. de C Hamilton and D. M. Wolpert, Sources of dignal-dependent noise during isometric force production, *J. Neurophysiol.* **88**(3) (2002) 1533–1544.
54. W. J. Kargo, Improvements in the Signal-to-Noise Ratio of Motor Cortex Cells Distinguish Early versus Late Phases of Motor Skill Learning, *J. Neurosci.* **24**(24) (2004) 5560–5569.
55. G. Barbati, C. Porcaro, F. Zappasodi *et al.*, Optimization of an independent component analysis approach for artifact identification and removal in magnetoencephalographic signals, *Clin. Neurophysiol.* **115**(5) (2004) 1220–1232.
56. C. Porcaro, M. T. Medaglia and A. Krott, Removing speech artifacts from electroencephalographic recordings during overt picture naming, *Neuroimage* **105** (2015) 171–180.
57. F. Tecchio, S. Graziadio, G. Barbati *et al.*, Somatosensory dynamic gamma-band synchrony: A neural code of sensorimotor dexterity, *Neuroimage* **35**(1) 185–193.
58. G. Barbati, R. Sigismondi, F. Zappasodi *et al.*, Functional source separation from magnetoencephalographic signals, *Hum. Brain Mapp.* **27**(12) (2006) 925–934.
59. G. Di Pino, C. Porcaro, M. Tombini *et al.*, A neurally-interfaced hand prosthesis tuned inter-hemispheric communication, *Restor. Neurol. Neurosci.* **30**(5) (2012) 407–418.
60. G. Barbati, C. Porcaro, A. Hadjipapas *et al.*, Functional source separation applied to induced visual gamma activity, *Hum. Brain Mapp* **29**(2) (2008) 131–141.
61. A. Hyvärinen, Fast and robust fixed-point algorithms for independent component analysis, *IEEE Trans. Neural Networks* **10**(3) (1999) 626–634.
62. F. Li, W. Peng, Y. Jiang *et al.*, The dynamic brain networks of motor imagery: Time-varying causality analysis of scalp EEG, *Int. J. Neural Syst.* **29**(1) (2019) 1850016.
63. D. Zhang, F. Xu, H. Xu *et al.*, Quantifying different tactile sensations evoked by cutaneous electrical stimulation using electroencephalography features, *Int. J. Neural Syst.* **26**(2) (2016) 1650006.
64. Y. Benjamini and Y. Hochberg, Controlling the false discovery rate: A practical and powerful approach to multiple testing , *J. R. Stat. Soc. Ser. B* **57**(1) (1995) 289–300.
65. S. Heuninckx, N. Wenderoth, S. P. Swinnen, Age-related reduction in the differential pathways involved in internal and external movement generation, *Neurobiol. Aging* **31**(2) (2010) 301–314.
66. K. A. Neely, P. J. Planetta, J. Prodoehl *et al.*, Force control deficits in individuals with parkinson's disease, multiple systems atrophy, and progressive supranuclear palsy, *PLoS One* **8**(3) (2013) e58403.
67. J. Prodoehl, P. J. Planetta, A. S. Kurani *et al.*, Differences in brain activation between tremor- and nontremor-dominant parkinson disease, *Arch. Neurol.* **70**(1) (2013) 100–106.

68. N. S. Ward, O. B. C. Swayne and J. M. Newton, Age-dependent changes in the neural correlates of force modulation: An fMRI study, *Neurobiol. Aging* **29**(9) (2008) 1434–1446.
69. E. López-Larraz, J. Ibáñez, F. Trincado-Alonso *et al.*, Comparing recalibration strategies for electroencephalography-based decoders of movement intention in neurological patients with motor disability, *Int. J. Neural Syst.* **28**(7) (2018) 1750060.
70. Y. Wang, M. Nakanishi and D. Zhang, EEG-based brain-computer interfaces, in *Adv. Exp. Med. Biol.* **1101** (2019) 41–65.
71. U. Chaudhary, N. Birbaumer and A. Ramos-Murguialday, Brain-computer interfaces for communication and rehabilitation, *Nat. Rev. Neurol.* **12**(9) (2016) 513–525.
72. S. D. Tabbal, M. Ushe, J. W. Mink *et al.*, Unilateral subthalamic nucleus stimulation has a measurable ipsilateral effect on rigidity and bradykinesia in parkinson disease, *Exp. Neurol.* **211**(1) (2008) 234–242.
73. R. J. Van Beers, P. Haggard and D. M. Wolpert, The role of execution noise in movement variability, *J. Neurophysiol.* **91**(2) (2004) 1050–1063.
74. S. Debener, M. Ullsperger, M. Siegel *et al.*, Trial-by-trial coupling of concurrent electroencephalogram and functional magnetic resonance imaging identifies the dynamics of performance monitoring, *J. Neurosci.* **25**(50) (2005) 11730–11737.
75. T. Eichele, K. Specht, M. Moosmann *et al.*, Assessing the spatiotemporal evolution of neuronal activation with single-trial event-related potentials and functional MRI, *Proc. Natl. Acad. Sci. USA* **102**(49) (2005) 17798–17803.
76. S. D. Mayhew, N. Hylands-White, C. Porcaro *et al.*, Intrinsic variability in the human response to pain is assembled from multiple, dynamic brain processes, *Neuroimage* **75** (2013) 68–78.
77. S. D. Mayhew, D. Ostwald, C. Porcaro and A. P. Bagshaw, Spontaneous EEG alpha oscillation interacts with positive and negative BOLD responses in the visual-auditory cortices and default-mode network, *Neuroimage* **76** (2013) 362–372.
78. A. Scaglione, K. A. Moxon, J. Aguilar, G. Foffani, Trial-to-trial variability in the responses of neurons carries information about stimulus location in the rat whisker thalamus, *Proc. Natl. Acad. Sci. USA* **108**(36) (2011) 14956–14961.
79. C. Scheibe, M. Ullsperger, W. Sommer, H. R. Heekeren, Effects of parametrical and trial-to-trial variation in prior probability processing revealed by simultaneous electroencephalogram/functional magnetic resonance imaging, *J. Neurosci.* **30**(49) (2010) 16709–16717.
80. Wu D Yu, G. Cai, Y. Yuan *et al.*, Application of nonlinear dynamics analysis in assessing unconsciousness: A preliminary study, *Clin. Neurophysiol.* **122**(3) (2011) 490–498.
81. S. Chettouf, L. M. Rueda-Delgado, R. de Vries *et al.*, Are unimanual movements bilateral? *Neurosci. Biobehav. Rev.* **113** (2020) 39–50.
82. H. J. Groenewegen, The basal ganglia and motor control, *Neural Plast.* **10**(1–2) (2003) 107–120.
83. M. A. Sommer, The role of the thalamus in motor control, *Curr. Opin. Neurobiol.* **13**(6) (2003) 663–670.
84. R. W. Guillery and S. M. Sherman, The thalamus as a monitor of motor outputs, *Phil. Trans. R. Soc. B*: *Biol. Sci.* **357** (2002) 1809–1821.